The FASEB Journal article fj.12-209841. Published online August 16, 2012.

Bone structure and B-cell populations, crippled by obesity, are partially rescued by brief daily exposure to low-magnitude mechanical signals

M. Ete Chan, Benjamin J. Adler, Danielle E. Green, and Clinton T. Rubin[1]

Department of Biomedical Engineering, Stony Brook University, Stony Brook, New York, USA

ABSTRACT **Deterioration of the immune and skeletal systems, each of which parallel obesity, reflects a fragile interrelationship between adiposity and osteoimmunology. Using a murine model of diet-induced obesity, this study investigated the ability of mechanical signals to protect the skeletal-immune systems at the tissue, cellular, and molecular level. A long-term (7 mo) high-fat diet increased total adiposity (+62%), accelerated age-related loss of trabecular bone (−61%), and markedly reduced B-cell number in the marrow (−52%) and blood (−36%) compared to mice fed a regular diet. In the final 4 mo of the protocol, the application of low-magnitude mechanical signals (0.2 g at 90 Hz, 15 min/d, 5 d/wk) restored both bone structure and B cells to those levels measured in control mice fed a regular diet. These phenotypic outcomes were achieved, in part, by reductions in osteoclastic activity and a biasing of hematopoietic stem cell differentiation toward the lymphoid B-cell lineage and away from a myeloid fate. These results emphasize that obesity undermines both the skeletal and immune systems, yet brief exposure to mechanical signals, perhaps as a surrogate to the salutary influence of exercise, diminishes the consequences of diabetes and obesity, restoring bone structure and normalizing B-cell populations by biasing of the fate of stem cells through mechanosensitive pathways.—Chan, M. E., Adler, B. J., Green, D. E., Rubin, C. T. Bone structure and B-cell populations, crippled by obesity, are partially rescued by brief daily exposure to low-magnitude mechanical signals. *FASEB J.* 26, 000–000 (2012). www.fasebj.org**

Key Words: adiposity · diabetes

Abbreviations: ALP, alkaline phosphatase; HFc, high-fat diet control; HSC, hematopoietic stem cell; HFv, high-fat diet + low-intensity vibration; LIV, low-intensity vibration; MSC, mesenchymal stem cell; PAX5, paired box 5; RANKL, receptor activator of nuclear factor κB ligand; RDc, regular diet control; RDv, regular diet + low-intensity vibration; SAT, subcutaneous adipose tissue; TAT, total adipose tissue; Tb.N, trabecular number; Tb.Sp, trabecular spacing; Tb.Th, trabecular thickness; TRAP, tartrate-resistant acid phosphatase; VAT, visceral adipose tissue

CONSEQUENCES OF OBESITY include type II diabetes (1), osteoporosis (2–8), and immune system dysfunction (9–11). Considering the close interactions between the immune and skeletal systems (12), it is plausible that an intervention effective in preserving bone mass may also help protect the immune system, ultimately reducing the severe systemic complications inherent to diabetes and obesity. As proof of principle in this regard, exercise has been shown to suppress obesity (13, 14), slow diabetes (15, 16), inhibit osteoporosis (17, 18), and strengthen the immune system (19). However, these salutary responses to this common "intervention" are most typically considered a generic, metabolic outcome of exertion (20), rather than a specific influence of mechanical signals on cell activity.

In some contrast to strenuous exercise, extremely low-magnitude mechanical signals have been shown to suppress adiposity (21, 22) and stimulate bone formation (23–25), to some degree by biasing mesenchymal stem cell (MSC) lineage selection toward osteoblastogenesis and away from adipogenesis (24). While this work has focused on mechanically driving the fate of MSCs, it is important to recognize that bone architecture is ultimately a product of both bone formation and bone resorption, the latter orchestrated through osteoclastogenesis and osteoclast activity (26–28). As the hematopoietic stem cell (HSC) is both the osteoclast and immune cell progenitor, and shares the bone marrow niche with the MSC, it becomes important to understand how obesity may perturb, and mechanical signals normalize, osteoclast activity and leukocyte distribution.

HSCs give rise to osteoclasts through the myeloid lineage, while lymphocytes such as B cells derive through the lymphoid pathway. Given the dichotomous early differentiation pathway of the HSC, an increased commitment toward one of these two lineages would inevitably decrease commitment toward the other. Indeed, obesity-related immune system dysfunction, as characterized by a reduction of immune cell proliferation and function (10, 11), may in some part be caused

[1] Correspondence: Department of Biomedical Engineering, Stony Brook University, Stony Brook, New York 11794-5281, USA. E-mail: clinton.rubin@sunysb.edu

doi: 10.1096/fj.12-209841

by a bias of HSC differentiation away from the lymphoid lineage and help explain the increase in osteoclasts *via* the myeloid lineage (2, 4), the result of which is an accelerated loss of trabecular bone (2, 6). In the study reported here, we examine the effect of diet-induced obesity on the skeletal and immune systems. Building on the demonstrated salutary effects of low-magnitude mechanical signals on adiposity (22) and MSCs (24), we investigate whether these signals, introduced into the obese animal, can bias HSC fate away from osteoclastogenesis and toward lymphopoiesis, ultimately helping to reestablish bone mass and restore the immune system.

MATERIALS AND METHODS

Experimental design

All animal protocols were reviewed and approved by the Stony Brook University Institutional Animal Care and Use Committee. This experiment consisted of two phases (**Fig. 1**), designed first to quantify the consequences of a high-fat diet on several physiological systems, and second to establish the capacity of low-intensity vibration (LIV) to mitigate any damage. Phase I started with twenty 2-mo old male C57BL/6J mice (Charles River, Wilmington, MA, USA), weight-matched, single-housed, and assigned to 4 groups: high-fat diet control (HFc); 2) high-fat diet + LIV (HFv); regular diet control (RDc); and regular diet + LIV (RDv) (n=5/group). Phase I employed a differential diet for 3 mo: Mice were fed either a regular or a high-fat diet (45% kcal from fat; van Heek Series 58V8; TestDiet, Richmond, IN, USA) *ad libitum*. In phase II, 4 mo in duration, RDv and HFv mice were subjected to LIV (0.2 *g*, 90 Hz sine wave, 15 min/d, 5 d/wk; where *g* is earth's gravitational field, or 9.8 m/s^2), delivered through a vertically oscillating platform (displacement ~100 μm; Marodyne, Lakeland, FL, USA). All animals in the HFc and RDc groups were sham handled by placing them on an inactive platform for the same period each day. Animal weight and food intake were monitored weekly, and spleen weight was measured at euthanasia.

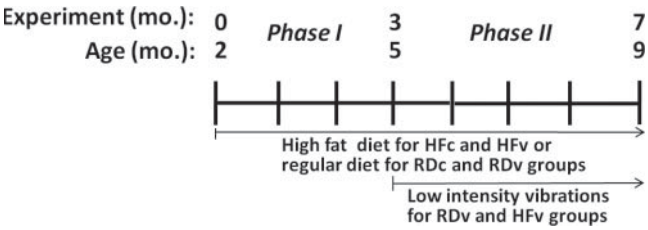

Figure 1. Timeline showing two phases of the experiment. Phase I, which began when the mice were 2 mo of age, involved only differences in diet: according to their assigned groups, mice were fed either a high-fat diet (HF) or a regular diet (RD) for 3 mo, allowing the obese phenotype to be fully established by 5 mo of age. Phase II then tested the effects of combined challenges of diet plus LIV in RDv and HFv groups, while RDc and HFc groups remained on the same diet treatment and were sham-loaded. While no differences were measured between RDc and RDv groups by the end of phase II, the obese phenotype created in the HFc group markedly accelerated bone loss between 5 and 9 mo of age, and suppressed the immune system, as indicated by compromised B-cell activity. HFv treatment, while slightly reducing adiposity relative to HFc treatment, served to restore the bone and reestablish B-cell levels to those in RD groups.

Quantification of adiposity and trabecular bone

Longitudinal *in vivo* measurements of fat and bone were performed for each animal at the end of phases I and II, using microcomputed tomography (μCT; vivaCT 40; Scanco Medical Inc., Brüttisellen, Switzerland). Calibration phantoms were scanned to establish accurate physical densities from the tissue linear attenuation values of the X-ray. The adipose tissue in the abdominal region (45 kV at 133 μA) and the trabecular bone in the proximal tibia (55 kV at 109 μA) were scanned at 76- and 17-μm isotropic resolution, respectively. Animals were positioned in a custom-designed holder and maintained under anesthesia (2% isoflurane) during the scanning period (29). The abdominal adipose tissue volume of the torso was quantified for the region spanning the proximal surface of the L1 vertebra through to the distal surface of L5 vertebra. The abdominal total adipose tissue (TAT) volume was further segregated into the individual volumes of visceral adipose tissue (VAT) and subcutaneous adipose tissue (SAT) and quantified using a custom automated algorithm (30, 31). The trabecular bone in the proximal tibial metaphysis (960 μm thickness, beginning 430 μm below the growth plate) was digitally segregated from the cortical bone and quantified for morphological parameters using a custom algorithm (32). The percentage change of trabecular and cortical bone parameters, which occurred over phase II, were evaluated for each individual animal.

Flow cytometric analysis of B and T cells in bone marrow and blood

At euthanasia, cellular constituents within the bone marrow were determined from the right femur. Bone marrow was flushed out of the cavity with supplemented medium, mixed, and filtered through a 70-μm mesh (BD Biosciences, San Jose, CA, USA). Supplemented medium was prepared with Dulbecco's modified essential medium (Life Technologies Inc., Gaithersburg, MD, USA), 2% fetal bovine serum (Invitrogen, Carlsbad, CA, USA), 1% penicillin/streptomycin, and 10 mM HEPES buffer (Life Technologies). Red blood cells in the bone marrow were lysed with 1× PharmLyse (BD Biosciences). A single-cell suspension containing 2×10^6 cells from each animal was prepared to identify the myeloid, T-, and B-cell populations through direct immunofluorescent staining with flow cytometeric analysis (FACSCalibur; BD Biosciences). B cells positive for B220 and T cells positive for CD4 and CD8 (33) were stained using fluorochrome-conjugated antibodies with distinct emission spectra [allophycocyanin (APC)- and phycoerythrin (PE)-conjugated CD45/B220 antibodies, and PE-conjugated CD4 and CD8 antibodies, respectively (BD Pharmingen; BD Biosciences)]. Similarly, 100 μl of whole blood obtained from cardiac puncture at euthanasia from all mice was lysed with 1× PharmLyse and prepared and stained for B- and T-cell populations, and characterized using FACS analysis software (FlowJo; Tree-Star, Inc., Ashland, OR, USA).

Bone resorption biomarker

Plasma isolated from the heparinized blood collected at euthanasia was portioned into aliquots and stored at −80°C until analysis. Using ELISA kits (Inter Medico, Markham, ON, Canada; MyBioSource, San Diego, CA, USA), the concentration of osteoclast-specific tartrate-resistant acid phosphatase

TABLE 1. *Summary of genes evaluated using real time RT-PCR to identify expression levels involved in HSC differentiation, B-cell lymphopoiesis, osteoclastogenesis and osteoclast activity*

Gene	Involvement	TaqMan gene expression assay
Nuclear factor of activated T-cells (Nfatc1)	Osteoclastogenesis	Mm00479445_m1
Peroxisome proliferator activated receptor γ (PPARγ)	Osteoclastogenesis	Mm01184322_m1
Paired box gene 5 (PAX5)	B lymphopoiesis	Mm00435501_m1
Tartrate-resistant acid phosphatase (TRAP)	Osteoclast development	Mm00475698_m1
Receptor activator of nuclear factor κB ligand (RANKL)	Osteoclast differentiation and activation	Mm01313944_g1

(TRAP)-5b and bone-specific alkaline phosphatase (ALP) in the plasma were measured and compared with standard curves according to manufacturer's instructions.

Gene expression in bone marrow

Total RNA was extracted from the bone marrow from the right tibia using the RNeasy Mini Kit (Qiagen, Valencia, CA, USA). Any DNA contamination was prevented by treatment with RNase free DNase (Qiagen). The extracted RNA was quantified and verified for its purity at an absorbance ratio of 260/280 with a spectrophotometer (NanoDrop; Thermo Scientific, Wilmington, DE, USA). A total of 400 ng of RNA from each sample was converted to single-stranded cDNA by a high-capacity cDNA reverse transcription kit (Applied Biosystems, Foster City, CA, USA). Aliquots of cDNA were stored at −20°C until analysis.

Gene expression levels of an array of genes, as summarized in **Table 1**, were evaluated using a real time PCR system (StepOnePlus; Applied Biosystems). Using TaqMan gene expression assays (Applied Biosystems), genes involved in B-cell lymphopoiesis [paired box 5 (PAX5); refs. 34, 35], osteoclastogenesis (Nfatc1, ref. 36; and PPARγ, refs. 37, 38) and bone resorption [TRAP, refs. 39, 40; and receptor activator of nuclear factor κB ligand (RANKL), refs. 41, 42] were analyzed. Standards and samples were normalized for the housekeeping gene 18s (TaqMan; Applied Biosystems), and all treatment groups were compared to RDc. In addition, any bias of the differentiation pathway of HSCs driven by the high-fat diet or the introduction of the mechanical signals toward either the osteoclast or B lymphocyte lineage was indicated by shifts in the ratios of Nfatc1:PAX5 and/or PPARγ:PAX5.

Statistical analysis

All data are shown as means ± SD. To determine significant differences between experimental groups, a 1-way analysis of variance (ANOVA) with a Tukey *post hoc* analysis was used. Statistical significance value was set at $P \leq 0.05$.

RESULTS

High-fat diet induced the obese phenotype

While several phenotypic responses in the HFc and HFv groups diverged over the phase II period, RDv treatment had no effect relative to RDc in any of the parameters considered, so these two RD groups were pooled for the presentation of the data. The HFv data are presented below, after first considering the effect of the HFc relative to RDc. By the end of the 3-mo high-fat-diet period, defined by the close of phase I, each HF group showed 37% higher body mass (**Fig. 2**) and 124% higher abdominal TAT volume when compared to the mice of the same age fed with a regular diet ($P<0.001$; **Fig. 3*A, B***). The 4-mo course of phase II showed a continued increase in body mass and adiposity across all groups, with the HFc group showing 45% higher body mass and 62% larger TAT volume than RD groups by the end of protocol ($P<0.001$). As compared to RDc, the higher adipose burden in the HFc group was caused predominately by an increase in VAT (+95%, $P<0.001$), as opposed to SAT (+12%, $P=0.43$) (Fig. 3*C, D*).

Obesity accelerated age-related loss of trabecular bone

Longitudinal evaluation of the proximal metaphysis of the tibia indicated that RD mice realized a loss of 38% of trabecular bone through the 4-mo period of phase II. This is significantly less than the bone deterioration measured in the HFc group, which fell 61% from the

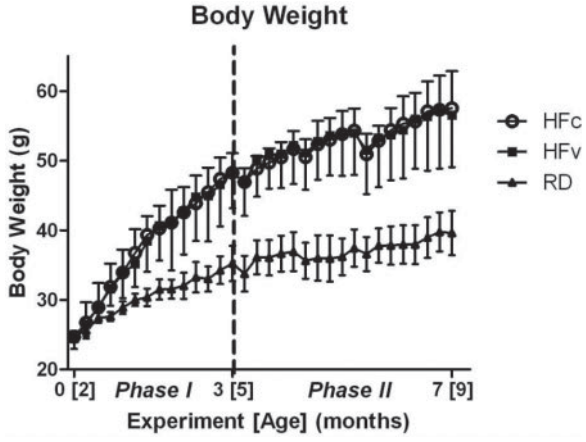

Figure 2. Change of body mass over two phases of the experiment. Phase I spanned 0 to 3 mo of the protocol, which brought mice from 2 to 5 mo of age. Phase II, beginning at dashed line, spanned 3 to 7 mo of the protocol, which brought mice from 5 to 9 mo of age. While marked increases in body mass between the HF and RD groups were found through the entire protocol, the mechanical intervention (RDv and HFv treatment) did not cause a divergence in mass from the control groups. Body mass of HF groups are significantly higher than RD groups starting at the fourth week, and extended through the remainder of the study.

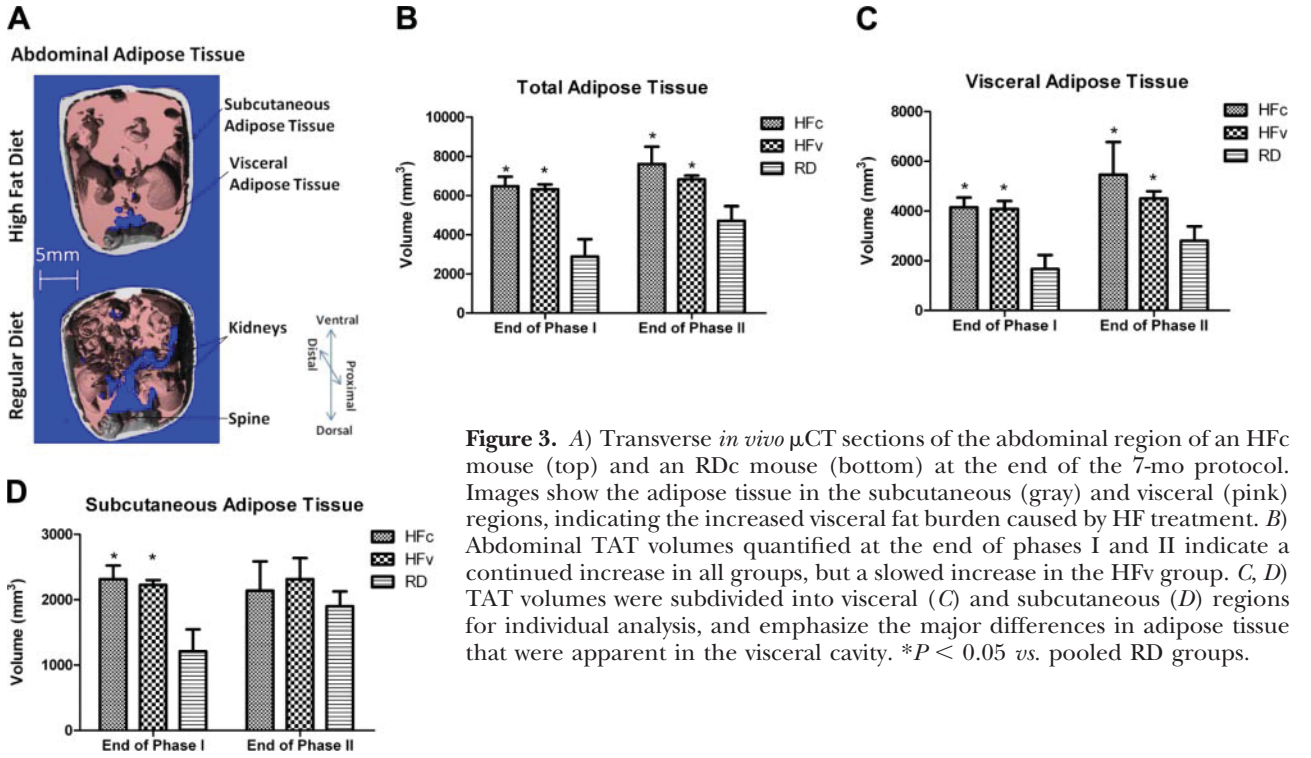

Figure 3. *A*) Transverse *in vivo* μCT sections of the abdominal region of an HFc mouse (top) and an RDc mouse (bottom) at the end of the 7-mo protocol. Images show the adipose tissue in the subcutaneous (gray) and visceral (pink) regions, indicating the increased visceral fat burden caused by HF treatment. *B*) Abdominal TAT volumes quantified at the end of phases I and II indicate a continued increase in all groups, but a slowed increase in the HFv group. *C*, *D*) TAT volumes were subdivided into visceral (*C*) and subcutaneous (*D*) regions for individual analysis, and emphasize the major differences in adipose tissue that were apparent in the visceral cavity. $^{*}P < 0.05$ *vs.* pooled RD groups.

baseline established at the beginning of phase II ($P<0.003$; **Fig. 4*A*, *B***). The microstructural changes of the trabecular bone in the RD groups showed that the age-related bone loss was realized through an aggregate of a 21% reduction of trabecular number (Tb.N), 11% thinning of trabecular thickness (Tb.Th), and 39% increase in trabecular separation (Tb.Sp; Fig. 4*C*). As compared to RD groups, the accelerated loss of bone volume in the HFc group was due to the product of a 289% reduction in Tb.Th, 27% loss in Tb.N, and 61% increase in Tb.Sp. No change in any individual microstructural parameter measured in HFc mice was significantly different from RD groups. Trabecular bone mineral density, cortical bone volume, or cortical bone mineral density was not affected by the high-fat diet. Relative to baseline, the slight decreases in trabecular bone mineral density in HFc mice (−3.5%, $P=0.36$) and RD mice (−1.3%, $P=0.51$) were not significantly different. In terms of cortical bone, neither HFc nor RD mice experienced significant changes in bone loss (−7%, $P=0.99$) and bone mineral density increased (+3%, $P=0.97$) relative to baseline (43).

Suppression of B-lymphocyte populations by obesity

Flow cytometry analysis indicated that both B- and T-cell populations were significantly repressed by the high-fat diet as compared to regular diet. The propor-

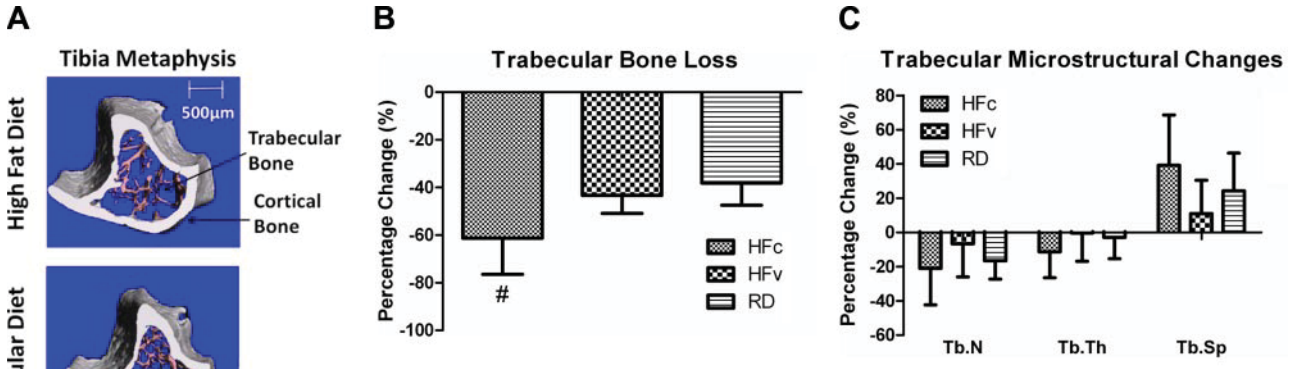

Figure 4. *A*) Reconstructed μCT images of the tibial metaphysis of a HFc (top) and RDc (bottom) mouse, showing the trabecular (pink) and cortical bone (gray) at the end of the 7 mo protocol. *B*) All mice experienced age-related trabecular bone loss from the end of phase I through the end of phase II, spanning 5 to 9 mo of age. However, HF treatment accelerated that bone loss in the HFc group, while the mechanical signals in HFv treatment restored values to those measured in the RD mice. *C*) Accelerated loss of bone in the HFc group was an aggregate of nonsignificant decreases in trabecular number (Tb.N) and thickness (Tb.Th), paralleled by increases in trabecular spacing (Tb.Sp). $^{\#}P < 0.05$ *vs.* HFv and pooled RD groups.

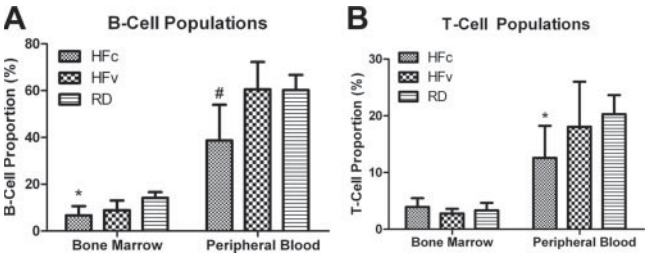

Figure 5. *A*) Flow cytometry analysis of the B-cell populations in bone marrow and peripheral blood, showing the detrimental effect of a long-term high-fat diet in HFc mice, as indicated by significant reduction in cell proportions relative to RD mice. The mechanical signal in HFv treatment restored the B-cell values such that they were not significantly different from RD groups. *B*) T-cell population of HFc mice exhibited significant reduction in the peripheral blood but not in the bone marrow, while HFv mice showed a trend toward recovery. $^{*}P < 0.05$ *vs.* RD groups; $^{\#}P < 0.05$ *vs.* HFv and pooled RD groups.

tion of B cells in the bone marrow of RD mice was 14%, and 60% in the peripheral blood (**Fig. 5*A***). HFc treatment resulted in significant reductions of B-cell populations both in the bone marrow (−52%, $P<0.05$) and in the blood (−36%, $P<0.01$) as compared to RD. While the spleen weights of HFc mice (+91%, $P=0.001$) and HFv mice (+68%, $P<0.02$) were higher than in RD groups, the spleen-to-body-weight ratios of HFc mice (+35%, $P=0.08$) and HFv mice (+20%, $P=0.52$) were not significantly higher than in RD groups. While T-cell proportions in the RD mice were 3 and 20% in the bone marrow and blood, respectively, the effect of HFc was mainly evident only in the blood, with 38% reduction in T-cell populations relative to RD groups ($P=0.05$, Fig. 5*B*).

Salutary effect of LIV on adipose, bone and B-cell status

While HFc treatment resulted in a 95% increase in VAT over RD ($P<0.001$), LIV attenuated VAT in HFv mice by −18%, making it only 60% higher than in RD mice ($P<0.02$; Fig. 3*C*). Also, while the amount of bone lost in HFc mice was significantly greater than RD, the 43% loss of trabecular bone in HFv mice over phase II was significantly less than in HFc mice (−29%, $P<0.05$) and resulted in a trabecular volume similar to the 38% loss measured in RD mice over phase II ($P=0.73$; Fig. 4*B*). Finally, while HFc treatment caused a significant reduction in B-cell proportion in the bone marrow and blood, circulating B cells in HFv mice were 57% higher than in HFc mice ($P<0.04$), restoring them to levels measured in the blood of RD mice (+1%, $P=0.99$; Fig. 5*A*). The 32% increase in B cells in the bone marrow of HFv mice was not significantly different than that measured in HFc mice.

Influence of high-fat diet and LIV on bone-resorption biomarker and gene expression

Circulating bone-resorption biomarker TRAP-5b levels increased by 30% in HFc mice as compared to RD mice ($P=0.02$), while LIV suppressed the TRAP-5b level of HFv mice by 7%, making it only 21% higher than in RD mice ($P>0.05$; **Fig. 6*A***). However, circulating bone-formation biomarker ALP only showed trends of reduction in HFc mice (−23%, $P=0.35$) and HFv mice (−2.1%, $P=0.99$) relative to RD mice. Real-time RT-PCR data showed that TRAP gene expression in HFc mice increased by 87% relative to RD mice ($P<0.03$). In some contrast, the 8% increase in TRAP measured in the marrow of HFv mice relative to RD mice was not significant ($P=0.97$; Fig. 6*B*). RANKL expression in the marrow indicated a trend of 69% up-regulation in HFc mice as compared to RD mice ($P=0.34$), and a trend of 66% reduction in HFv mice relative to HFc mice ($P=0.17$). Compared to RD mice, HFc mice showed trends of 41 and 61% up-regulation in Nfatc1 and PPARγ expression, respectively, and a trend of 29% down-regulation of PAX5 expression (**Fig. 7*A***). Conversely, HFv mice showed trends of 19 and 34% lower Nfatc1 and PPARγ expression, respectively, and a trend of 20% higher PAX5 expression relative to HFc mice.

As an indication of the commitment bias of stem cells toward either osteoclasts in the myeloid lineage or B cells in the lymphoid lineage, HFc mice displayed 133% increase in the Nfatc1:PAX5 ratio ($P<0.04$) as compared to RD mice, whereas HFv mice indicated a nonsignificant 77% increase ($P=0.76$; Fig. 7*B*). Similarly, the PPARγ:PAX5 ratio in HFc mice was 155% higher than in RD mice ($P<0.01$), while HFv mice

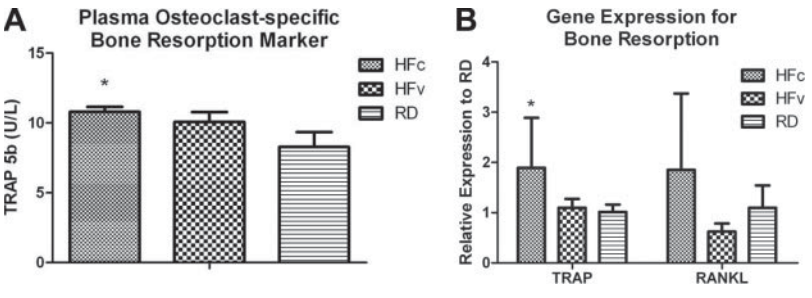

Figure 6. Acceleration and mitigation of bone loss by HF and LIV treatment, respectively, were further investigated at the molecular and transcriptional levels. Analysis of the plasma level of osteoclast-specific bone resorption biomarker TRAP-5b using ELISA (*A*) and expression levels of bone-resorption genes TRAP and RANKL using real-time rt-PCR (*B*) commonly showed up-regulation in the HFc compared to RD groups, indicating a contributing mechanism toward the accelerated loss of trabecular bone. Mechanical stimulation in the HFv group attenuated gene expression and bone-resorption biomarker for bone resorption, which may in part explain the rescue of trabecular bone relative to the RD mice. $^{*}P < 0.05$ *vs.* pooled RD groups.

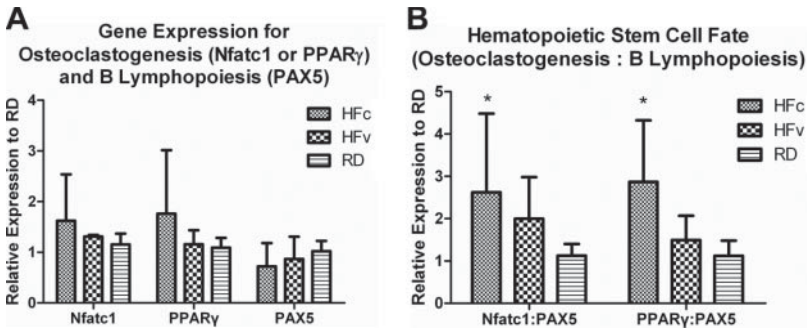

Figure 7. Osteoclasts and B lymphocytes share the same HSC progenitors in the bone marrow niche. *A*) Elevated expression of Nfatc1 and PPARγ indicated increased osteoclastogenesis, while lower PAX5 expression indicated reduced B lymphopoiesis in HFc relative to RD groups. *B*) Relative ratio of gene expression involved in osteoclastogenesis to B lymphopoiesis indicated how a long-term high-fat diet significantly biased HSC differentiation toward an osteoclast lineage and away from B-cell lineage in HFc compared to RD groups, while LIV ameliorated such obesity-induced bias of HSC differentiation in HFv group. $*P < 0.05$ *vs.* pooled RD groups.

indicated a nonsignificant 33% increase over RD mice (P=0.76).

DISCUSSION

Consequences of obesity include increased susceptibility to disease (1, 44) and vulnerability to skeletal fracture due to insufficient bone quality relative to the loads placed on them (3, 7). Using an *in vivo* animal model of diet-induced obesity, the data presented here indicate that obesity markedly accelerates the age-related deterioration of bone structure and simultaneously undermines the B-cell population as measured in both the marrow and blood. Recognizing the generic benefits of exercise on suppressing obesity, strengthening immunity, and reversing osteopenia, the data from these experiments indicate that extremely low-magnitude mechanical signals, independent of reducing obesity *per se*, helped to reestablish the B-cell population and restore the bone structure despite a continued metabolic insult of a sustained high-fat diet. That the mechanical signals were so subtle, and applied for such a brief period of time, suggests that these salutary outcomes were achieved in part through a mechanically mediated shift in the fate selection of HSCs, suppressing osteoclastogenesis and restoring B-cell lymphopoiesis.

Building from previous work with this model, where the ability of these low-magnitude mechanical signals to suppress adiposity was evaluated (24), here we investigate the capacity of this stimulus to influence bone and immune system outcomes in mice that were already obese, a phenotype established in phase I of the protocol. By the end of phase II, the HFc mice were significantly fatter and heavier than RD mice, whereas exposure to the LIV signal caused a slight reduction of adipose tissue in the visceral compartment in the HFv mice, while no effect was seen in the subcutaneous region. Notably, VAT is known to be more predictive of obesity-induced pathologies, such as type 2 diabetes and coronary heart disease, than either the total or subcutaneous adiposity alone (45–47). Further, VAT has been shown as negatively correlated to bone mineral density of the appendicular and axial skeleton (48). Importantly, previous work has shown that the activities and metabolism indices of the mice subject to LIV, including during the time the stimulus was delivered, were essentially identical to the sham-handled mice (49), revealing a metabolically independent, mechanotransduction pathway that reduces the visceral adipose burden over time.

As compared to that measured at the end of phase I, when the mice were 5 mo of age, a significant decline in bone quality and quantity was found over the subsequent 4 mo in RD animals, at which point they were 9 mo of age. This loss reflects the well-recognized process of age-related decline in skeletal structure (50–52). The absence of any influence of the mechanical intervention on these "healthy" RD animals suggests that the LIV signal failed to influence physiological systems that were not in a disrupted state in the first place (53, 54). In some contrast, the skeletal system of the HFc mice indicated an accelerated loss of bone, doubling the rate at which bone disappeared compared to the age-matched, RD animals. These data emphasize the skeletal consequences of obesity; that it is not "simply" an undersized structure relative to the mechanical demands placed on it but that an active, catabolic process occurs in bone that far exceeds that measured in healthy aging mice, contributing to a compromised structure and an increased susceptibility to fracture (3, 7). In contrast, the LIV signal introduced to the HFv animals at the start of the 4-mo phase II reestablished bone architecture to those levels retained in RD mice. These data indicate that the consequences of obesity on accelerating the decline of the skeletal system are not necessarily inevitable and that a means of protecting or even rescuing bone structure exists despite a continued adipose burden.

In an effort to better understand the cellular and molecular mechanisms by which bone loss was accelerated in the HFc mice, we found that the plasma bone-resorption biomarker TRAP-5b, and gene expressions of TRAP and RANKL in the bone marrow of HF mice increased relative to RD mice, suggesting that the obese condition predisposes the marrow niche to be catabolic to bone. A recent *in vitro* study showed that, when subjected to a similar LIV protocol as the one used here (0.3 g; 30, 60 or 90 Hz; 1 h), osteocytes released significantly lower-soluble RANKL, which in turn inhibited the formation of multinucleated oste-

oclasts while attenuating the amount of resorptive activity (55). The suppression of TRAP and RANKL expression by LIV in the HFv group suggests a means, independent of promoting osteoblastogenesis (56), that drives bone turnover toward protecting the skeleton by biasing HSC progenitors away from osteoclastogenesis.

In addition to the accelerated loss of bone caused by HF treatment, the immune system was also compromised by obesity, as reflected by the significant reduction of B cells in HFc mice relative to RD mice. The decrease in both bone marrow and circulating B cells indicates an impairment of hematopoiesis, which may expose the host to a greater susceptibility to infection and a host of other diseases (11, 44). Restoration of the B-cell population in the HFv mice to RD levels through LIV suggests that mechanical signals, whether direct or introduced using exercise, serve to protect the immune system and that recovery from the disruption caused by obesity does not inherently require a reduction in adiposity but rather reestablishing healthy fate selection of the HSC progenitors. Ultimately, this finding suggests that the HSC population can be influenced directly by physical signals and that mechanical events can protect the adult stem cells from dysfunction even under the pressures of adipogenic conditions (56). Of course, further studies are essential to evaluate the functional performance of B cells in the HFc and HFv groups. Also, although C57BL/6J mice are a widely used model of diet-induced obesity as they develop similar pathologies as humans (*e.g.*, hyperglycemia and hyperinsulinemia) when subjected to a high-fat diet, differences in genetic background in a different obesity model could exhibit a distinct immune response.

As indicated by the HF-induced shift in gene expression ratios of PPARγ:PAX5 and Nfatc1:PAX5, obesity predisposed HSC differentiation toward osteoclastogenesis and away from B lymphopoiesis. Considering that PPARγ and Nfatc1 are both involved in osteoclastogenesis (36–38), while PAX5 is critical to B lymphopoiesis (34, 35), the 2-fold rise in these ratios caused by HF treatment provide some mechanistic insight into the fall in bone quality and collapse in B-cell numbers. Recent evidence also indicates that PPARγ, in addition to its accepted role in promoting adipogenesis and inhibiting osteoblastogenesis in MSCs, stimulates osteoclast differentiation from HSCs (37, 38). *In vivo* work studying the role of Nfatc1 in osteoclastogenesis demonstrates that the deletion of Nfatc1 in young mice resulted in osteopetrosis and inhibition of osteoclastogenesis (36). Also, Nfatc1 regulates RANKL-induced osteoclast activation by up-regulating osteoclast-activating genes, such as cathepsin K and c-Src (42). PAX5, an essential transcription factor in B-lineage commitment, works by suppressing alternative lineage choices (34). It is expressed exclusively in the B-lymphocyte lineage, essential for the commitment of lymphoid progenitors to the B-lymphocyte fate (35).

Interestingly, the application of LIV to the HFv group restored these ratios toward those measured in RD groups, which paralleled the rescue of B-cell populations and slowing of bone loss (Fig. 7*B*). This interpretation is supported by a series of studies that used a genetic-knockout model, $PAX5^{-/-}$ mice, where the PAX5 deficit was shown to cause not only a developmental arrest of B-cell lineage but also an osteopenia phenotype and an increase in osteoclast number (57). Extrapolating to the experiments reported here, the accelerated loss of bone and reduction in B cells as caused by the high-fat diet, coincident with a disruption of HSC differentiation, were similar in fashion to that measured in $PAX5^{-/-}$ mice, suggesting a key role for this gene in driving the phenotypic outcomes of diet-induced obesity, in terms of adipose burden, skeletal quality, and the balance of the immune system.

In summary, this study demonstrates that obesity will negatively affect both the skeletal and immune systems, and disrupt the balance of the bone marrow stem cell environment. Building on evidence that exercise helps to suppress obesity, reverse osteopenia, and strengthen immunity, the data presented here also indicate that brief daily exposure to extremely low-magnitude mechanical signals slowed the loss of bone and restored B-cell populations, despite the persistent insult caused by a high-fat diet. The rescue of the bone and B-cell systems toward that measured in RD groups was achieved in part by biasing the differentiation pathways of the hematopoietic stem cell toward lymphoid B-cell fate and away from osteoclastogenesis. Understanding the role of the stem cell niche in promulgating obesity-related disorders, and the salutary action of mechanical signals, may ultimately contribute to a unique nondrug treatment strategy for a host of diabetes- and obesity-related health problems. FJ

This work was supported by the U.S. National Institutes of Health through National Institute of Arthritis and Musculoskeletal and Skin Diseases grant AR043498. The authors are grateful for the help from Gunes Uzer, Ada Tsoi, Mario Botros, Elizabeth Fievisohn, Michelle Cheung, Kim Kawatra, and Engin Ozcivici for their technical assistance related to this project. Conflict of interest: C.T.R. is a founder of Marodyne Medical, Inc. (Lakeland, FL, USA) and has a U.S. Patent and Trademark Office application under review for the ability of mechanical signals to control metabolic disorders. The other authors declare no conflicts of interest.

REFERENCES

1. Kahn, S. E., Zinman, B., Haffner, S. M., O'Neill, M. C., Kravitz, B. G., Yu, D., Freed, M. I., Herman, W. H., Holman, R. R., Jones, N. P., Lachin, J. M., and Viberti, G. C. (2006) Obesity is a major determinant of the association of C-reactive protein levels and the metabolic syndrome in type 2 diabetes. *Diabetes* **55,** 2357–2364
2. Cao, J. J., Sun, L., and Gao, H. (2010) Diet-induced obesity alters bone remodeling leading to decreased femoral trabecular bone mass in mice. *Ann. N. Y. Acad. Sci.* **1192,** 292–297
3. Compston, J. E., Watts, N. B., Chapurlat, R., Cooper, C., Boonen, S., Greenspan, S., Pfeilschifter, J., Silverman, S., Diez-Perez, A., Lindsay, R., Saag, K. G., Netelenbos, J. C., Gehlbach, S., Hooven, F. H., Flahive, J., Adachi, J. D., Rossini, M., Lacroix, A. Z., Roux, C., Sambrook, P. N., and Siris, E. S. (2011) Obesity

is not protective against fracture in postmenopausal women: GLOW. *Am. J. Med.* **124,** 1043–1050
4. Halade, G. V., El Jamali, A., Williams, P. J., Fajardo, R. J., and Fernandes, G. (2011) Obesity-mediated inflammatory microenvironment stimulates osteoclastogenesis and bone loss in mice. *Exp. Gerontol.* **46,** 43–52
5. Halade, G. V., Rahman, M. M., Williams, P. J., and Fernandes, G. (2010) High fat diet-induced animal model of age-associated obesity and osteoporosis. *J. Nutr. Biochem.* **21,** 1162–1169
6. Patsch, J. M., Kiefer, F. W., Varga, P., Pail, P., Rauner, M., Stupphann, D., Resch, H., Moser, D., Zysset, P. K., Stulnig, T. M., and Pietschmann, P. (2011) Increased bone resorption and impaired bone microarchitecture in short-term and extended high-fat diet-induced obesity. *Metabolism* **60,** 243–249
7. Premaor, M. O., Ensrud, K., Lui, L., Parker, R. A., Cauley, J., Hillier, T. A., Cummings, S., and Compston, J. E. (2011) Risk factors for nonvertebral fracture in obese older women. *J. Clin. Endocrinol. Metab.* **96,** 2414–2421
8. Rosen, C. J., and Klibanski, A. (2009) Bone, fat, and body composition: evolving concepts in the pathogenesis of osteoporosis. *Am. J. Med.* **122,** 409–414
9. Crevel, R. W., Friend, J. V., Goodwin, B. F., and Parish, W. E. (1992) High-fat diets and the immune response of C57Bl mice. *Br. J. Nutr.* **67,** 17–26
10. O'Rourke, R. W., Kay, T., Scholz, M. H., Diggs, B., Jobe, B. A., Lewinsohn, D. M., and Bakke, A. C. (2005) Alterations in T-cell subset frequency in peripheral blood in obesity. *Obes. Surg.* **15,** 1463–1468
11. Sato Mito, N., Suzui, M., Yoshino, H., Kaburagi, T., and Sato, K. (2009) Long term effects of high fat and sucrose diets on obesity and lymphocyte proliferation in mice. *J. Nutr. Health Aging* **13,** 602–606
12. Takayanagi, H. (2007) Osteoimmunology: shared mechanisms and crosstalk between the immune and bone systems. *Nat. Rev. Immunol.* **7,** 292–304
13. Barbeau, P., Johnson, M. H., Howe, C. A., Allison, J., Davis, C. L., Gutin, B., and Lemmon, C. R. (2007) Ten months of exercise improves general and visceral adiposity, bone, and fitness in black girls. *Obesity* **15,** 2077–2085
14. Gutin, B. (2008) Child obesity can be reduced with vigorous activity rather than restriction of energy intake. *Obesity* **16,** 2193–2196
15. Eriksson, K. F., and Lindgarde, F. (1991) Prevention of type 2 (non-insulin-dependent) diabetes mellitus by diet and physical exercise. The 6-year Malmo feasibility study. *Diabetologia* **34,** 891–898
16. Pan, X., Li, G., and Hu, Y. (1995) [Effect of dietary and/or exercise intervention on incidence of diabetes in 530 subjects with impaired glucose tolerance (from 1986–1992)]. *Zhonghua Nei Ke Za Zhi* **34,** 108–112
17. Dilsen, G., Berker, C., Oral, A., and Varan, G. (1989) The role of physical exercise in prevention and management of osteoporosis. *Clin. Rheumatol.* **8**(Suppl. 2), 70–75
18. Tolomio, S., Ermolao, A., Lalli, A., and Zaccaria, M. (2010) The effect of a multicomponent dual-modality exercise program targeting osteoporosis on bone health status and physical function capacity of postmenopausal women. *J. Women Aging* **22,** 241–254
19. Zhou, Q., Leeman, S. E., and Amar, S. (2011) Signaling mechanisms in the restoration of impaired immune function due to diet-induced obesity. *Proc. Natl. Acad. Sci. U. S. A.* **108,** 2867–2872
20. Thivel, D., Isacco, L., Rousset, S., Boirie, Y., Morio, B., and Duche, P. (2011) Intensive exercise: a remedy for childhood obesity? *Physiol. Behav.* **102,** 132–136
21. Luu, Y. K., Ozcivici, E., Capilla, E., Adler, B., Chan, E., Shroyer, K., Rubin, J., Judex, S., Pessin, J. E., and Rubin, C. T. (2010) Development of diet-induced fatty liver disease in the aging mouse is suppressed by brief daily exposure to low-magnitude mechanical signals. *Int. J. Obes. (Lond.)* **34,** 401–405
22. Rubin, C. T., Capilla, E., Luu, Y. K., Busa, B., Crawford, H., Nolan, D. J., Mittal, V., Rosen, C. J., Pessin, J. E., and Judex, S. (2007) Adipogenesis is inhibited by brief, daily exposure to high-frequency, extremely low-magnitude mechanical signals. *Proc. Natl. Acad. Sci. U. S. A.* **104,** 17879–17884
23. Judex, S., Lei, X., Han, D., and Rubin, C. (2007) Low-magnitude mechanical signals that stimulate bone formation in the ovariectomized rat are dependent on the applied frequency but not on the strain magnitude. *J. Biomech.* **40,** 1333–1339
24. Luu, Y. K., Capilla, E., Rosen, C. J., Gilsanz, V., Pessin, J. E., Judex, S., and Rubin, C. T. (2009) Mechanical stimulation of mesenchymal stem cell proliferation and differentiation promotes osteogenesis while preventing dietary-induced obesity. *J. Bone Miner. Res.* **24,** 50–61
25. Ozcivici, E., Luu, Y. K., Rubin, C. T., and Judex, S. (2010) Low-level vibrations retain bone marrow's osteogenic potential and augment recovery of trabecular bone during reambulation. *PLoS One* **5,** e11178
26. Blair, H. C. (1998) How the osteoclast degrades bone. *Bioessays* **20,** 837–846
27. Dodds, R. A., Connor, J. R., James, I. E., Rykaczewski, E. L., Appelbaum, E., Dul, E., and Gowen, M. (1995) Human osteoclasts, not osteoblasts, deposit osteopontin onto resorption surfaces: an in vitro and ex vivo study of remodeling bone. *J. Bone Min. Res.* **10,** 1666–1680
28. Jilka, R. L., Weinstein, R. S., Takahashi, K., Parfitt, A. M., and Manolagas, S. C. (1996) Linkage of decreased bone mass with impaired osteoblastogenesis in a murine model of accelerated senescence. *J. Clin. Invest.* **97,** 1732–1740
29. Judex, S., Luu, Y. K., Ozcivici, E., Adler, B., Lublinsky, S., and Rubin, C. T. (2010) Quantification of adiposity in small rodents using micro-CT. *Methods* **50,** 14–19
30. Lublinsky, S., Luu, Y. K., Rubin, C. T., and Judex, S. (2009) Automated separation of visceral and subcutaneous adiposity in in vivo microcomputed tomographies of mice. *J. Digit. Imaging* **22,** 222–231
31. Luu, Y. K., Lublinsky, S., Ozcivici, E., Capilla, E., Pessin, J. E., Rubin, C. T., and Judex, S. (2009) In vivo quantification of subcutaneous and visceral adiposity by micro-computed tomography in a small animal model. *Med. Eng. Phys.* **31,** 34–41
32. Lublinsky, S., Ozcivici, E., and Judex, S. (2007) An automated algorithm to detect the trabecular-cortical bone interface in micro-computed tomographic images. *Calcif. Tissue Int.* **81,** 285–293
33. Weksberg, D. C., Chambers, S. M., Boles, N. C., and Goodell, M. A. (2008) CD150- side population cells represent a functionally distinct population of long-term hematopoietic stem cells. *Blood* **111,** 2444–2451
34. Nutt, S. L., Heavey, B., Rolink, A. G., and Busslinger, M. (1999) Commitment to the B-lymphoid lineage depends on the transcription factor Pax5. *Nature* **401,** 556–562
35. Urbanek, P., Wang, Z. Q., Fetka, I., Wagner, E. F., and Busslinger, M. (1994) Complete block of early B cell differentiation and altered patterning of the posterior midbrain in mice lacking Pax5/BSAP. *Cell* **79,** 901–912
36. Aliprantis, A. O., Ueki, Y., Sulyanto, R., Park, A., Sigrist, K. S., Sharma, S. M., Ostrowski, M. C., Olsen, B. R., and Glimcher, L. H. (2008) NFATc1 in mice represses osteoprotegerin during osteoclastogenesis and dissociates systemic osteopenia from inflammation in cherubism. *J. Clin. Invest.* **118,** 3775–3789
37. Wan, Y., Chong, L. W., and Evans, R. M. (2007) PPAR-gamma regulates osteoclastogenesis in mice. *Nat. Med.* **13,** 1496–1503
38. Wei, W., Wang, X., Yang, M., Smith, L. C., Dechow, P. C., Sonoda, J., Evans, R. M., and Wan, Y. (2010) PGC1beta mediates PPARgamma activation of osteoclastogenesis and rosiglitazone-induced bone loss. *Cell Metab.* **11,** 503–516
39. Hollberg, K., Hultenby, K., Hayman, A., Cox, T., and Andersson, G. (2002) Osteoclasts from mice deficient in tartrate-resistant acid phosphatase have altered ruffled borders and disturbed intracellular vesicular transport. *Exp. Cell Res.* **279,** 227–238
40. Lindunger, A., MacKay, C. A., Ek-Rylander, B., Andersson, G., and Marks, S. C., Jr. (1990) Histochemistry and biochemistry of tartrate-resistant acid phosphatase (TRAP) and tartrate-resistant acid adenosine triphosphatase (TrATPase) in bone, bone marrow and spleen: implications for osteoclast ontogeny. *Bone Miner.* **10,** 109–119
41. Ominsky, M. S., Stouch, B., Schroeder, J., Pyrah, I., Stolina, M., Smith, S. Y., and Kostenuik, P. J. (2011) Denosumab, a fully human RANKL antibody, reduced bone turnover markers and increased trabecular and cortical bone mass, density, and strength in ovariectomized cynomolgus monkeys. *Bone* **49,** 162–173

42. Song, I., Kim, J. H., Kim, K., Jin, H. M., Youn, B. U., and Kim, N. (2009) Regulatory mechanism of NFATc1 in RANKL-induced osteoclast activation. *FEBS Lett.* **583,** 2435–2440
43. Cao, J. J., Gregoire, B. R., and Gao, H. (2009) High-fat diet decreases cancellous bone mass but has no effect on cortical bone mass in the tibia in mice. *Bone* **44,** 1097–1104
44. Reilly, J. J., and Kelly, J. (2011) Long-term impact of overweight and obesity in childhood and adolescence on morbidity and premature mortality in adulthood: systematic review. *Int. J. Obes. (Lond.)* **35,** 891–898
45. Fox, C. S., Massaro, J. M., Hoffmann, U., Pou, K. M., Maurovich-Horvat, P., Liu, C. Y., Vasan, R. S., Murabito, J. M., Meigs, J. B., Cupples, L. A., D'Agostino, R. B., Sr., and O'Donnell, C. J. (2007) Abdominal visceral and subcutaneous adipose tissue compartments: association with metabolic risk factors in the Framingham Heart Study. *Circulation* **116,** 39–48
46. Haffner, S. M. (2007) Abdominal adiposity and cardiometabolic risk: do we have all the answers? *Am. J. Med.* **120,** S10–S16; discussion S16–S17
47. Taguchi, R., Takasu, J., Itani, Y., Yamamoto, R., Yokoyama, K., Watanabe, S., and Masuda, Y. (2001) Pericardial fat accumulation in men as a risk factor for coronary artery disease. *Atherosclerosis* **157,** 203–209
48. Russell, M., Mendes, N., Miller, K. K., Rosen, C. J., Lee, H., Klibanski, A., and Misra, M. (2010) Visceral fat is a negative predictor of bone density measures in obese adolescent girls. *J. Clin. Endocrinol. Metab.* **95,** 1247–1255
49. Judex, S., and Rubin, C. T. (2010) Is bone formation induced by high-frequency mechanical signals modulated by muscle activity? *J. Musculoskelet. Neuronal Interact.* **10,** 3–11
50. Ferguson, V. L., Ayers, R. A., Bateman, T. A., and Simske, S. J. (2003) Bone development and age-related bone loss in male C57BL/6J mice. *Bone* **33,** 387–398
51. Ferguson, V. L., Greenberg, A. R., Bateman, T. A., Ayers, R. A., and Simske, S. J. (1999) The effects of age and dietary restriction without nutritional supplementation on whole bone structural properties in C57BL/6J mice. *Biomed. Sci. Instrum.* **35,** 85–91
52. Halloran, B. P., Ferguson, V. L., Simske, S. J., Burghardt, A., Venton, L. L., and Majumdar, S. (2002) Changes in bone structure and mass with advancing age in the male C57BL/6J mouse. *J. Bone Min. Res.* **17,** 1044–1050
53. Rubin, C., Recker, R., Cullen, D., Ryaby, J., McCabe, J., and McLeod, K. (2004) Prevention of postmenopausal bone loss by a low-magnitude, high-frequency mechanical stimuli: a clinical trial assessing compliance, efficacy, and safety. *J. Bone Miner. Res.* **19,** 343–351
54. Slatkovska, L., Alibhai, S. M., Beyene, J., Hu, H., Demaras, A., and Cheung, A. M. (2011) Effect of 12 months of whole-body vibration therapy on bone density and structure in postmenopausal women: a randomized trial. *Ann. Intern. Med.* **155,** 668–679, W205
55. Lau, E., Al-Dujaili, S., Guenther, A., Liu, D., Wang, L., and You, L. (2010) Effect of low-magnitude, high-frequency vibration on osteocytes in the regulation of osteoclasts. *Bone* **46,** 1508–1515
56. Sen, B., Guilluy, C., Xie, Z., Case, N., Styner, M., Thomas, J., Oguz, I., Rubin, C., Burridge, K., and Rubin, J. (2011) Mechanically induced focal adhesion assembly amplifies anti-adipogenic pathways in mesenchymal stem cells. *Stem Cells* **29,** 1829–1836
57. Horowitz, M. C., Xi, Y., Pflugh, D. L., Hesslein, D. G., Schatz, D. G., Lorenzo, J. A., and Bothwell, A. L. (2004) Pax5-deficient mice exhibit early onset osteopenia with increased osteoclast progenitors. *J. Immunol.* **173,** 6583–6591

Received for publication April 16, 2012.
Accepted for publication August 6, 2012.